

Banner appropriate to article type will appear here in typeset article

# Investigation of hydrogen under-expanded jets in gaseous propulsion systems

Francesco Duronio<sup>1 2 †</sup>, and Andrea Di Mascio<sup>1</sup>

<sup>1</sup>Dipartimento di Ingegneria Industriale Informazione e di Economia - Università degli studi dell'Aquila Piazzale Ernesto Pontieri, Monteluco di Roio, 67100, L'Aquila (AQ), Italy

<sup>2</sup>Consiglio Nazionale delle Ricerche, Istituto di Scienze e Tecnologie per l'Energia e la Mobilità Sostenibili (STEMS), Via G. Marconi 4, 80125 Napoli, Italy

(Received xx; revised xx; accepted xx)

Underexpanded jets are present in various engineering applications; in recent years, they have gained special attention because of the development of gaseous-fueled propulsion systems. In these apparatuses, the direct injection of fuels such as hydrogen in innovative low-emission engines' chambers induces turbulent under-expanded jets. In this study, we performed high-fidelity Large Eddy Simulations of under-expanded hydrogen jets to investigate these flows and provide valuable insights for developing injectors suitable for hydrogen and, more generally, gaseous-fueled propulsion systems. We initially assessed the method's accuracy, evaluating the convergence and uncertainty of the numerical results and validating them against experimental particle image velocimetry and Schlieren data. The simulated jets, the Mach disc dimensions, and the resulting velocity field align closely with the experimental observations. Then we analyzed the jet structure for pressure ratios of 4 to 25 and examined the effects of the geometrical configuration of the nozzle on the characteristics of the air-fuel mixture obtained. We compared the jets resulting from a round-hole nozzle with annular ones resembling outward-opening injectors.

## 1. Introduction

Under-expanded jets are complex high-speed flows in multiple engineering applications, such as exhaust plumes from aircraft, rockets, missiles, and combustion chambers. Additionally, these jets can occur in natural phenomena, like volcanic eruptions (Orescanin *et al.* 2010; von der Linden *et al.* 2021; Carcano *et al.* 2013; FOX 1974). Consequently, under-expanded jets have been extensively studied, particularly in aerospace applications. However, in the past decade, research has focused more and more on their role in the injection process of advanced propulsion systems, positioning this as an emerging field within fluid dynamics and engine simulations (Duronio *et al.* 2023, 2021). Therefore, it is crucial to develop a comprehensive understanding of these processes for propulsion systems (Onorati *et al.* 2022).

Modern propulsion systems often adopt gases such as hydrogen, propane, ammonia, and methane rather than liquids. Due to the significant pressure difference between the injector rail and the injection environment, supersonic conditions are achieved (Duronio *et al.* 2023; Vuorinen *et al.* 2014; Hamzehloo & Aleiferis 2014*b*, 2016*b*), with the formation

† Email address for correspondence: francesco.duronio@univaq.it

of underexpanded jets downstream of the injector nozzles, resulting in a distinctive flow field structure (Allocca *et al.* 2020; Samsam-Khayani *et al.* 2022).

Among the different combustibles, hydrogen is the subject of the most attention and research efforts; in this context, direct injection into the combustion chamber is one of the most promising technologies. Of course, the injection process plays a relevant role in the chain of events that take place in a propulsion system. Consequently, we must investigate the injectors and the resulting under-expanded jets to obtain the desired air-fuel mixture, efficient combustion, and reduced tailpipe emissions.

In recent years, researchers have focused their investigation on methane jets (Yosri *et al.* 2020; Banholzer *et al.* 2019; Bartolucci *et al.* 2020; Dong *et al.* 2018); comparatively less attention has been paid to hydrogen fuel, despite its growing scientific relevance. Experimental investigation exploits Schlieren imaging to capture the evolution of transient under-expanded hydrogen jets from gaseous fuel injectors, evaluating factors such as pressure ratio (PR), nozzle characteristics, and jet tip penetration (Coratella *et al.* 2024; Yeganeh *et al.* 2023a; Lee *et al.* 2021; Yeganeh *et al.* 2023b, 2022). Unlike jets of other species, examined using density maps and planar laser-induced fluorescence (PLIF), providing local values of fuel concentration and gas density (Yu *et al.* 2013b, 2011; Sakellarakis *et al.* 2021; Ni *et al.* 2022), experimental studies on hydrogen jets are often limited to qualitative observations, although detailed investigations are crucial for robust validation of new methods and CFD simulations of under-expanded jets.

Considering the intrinsic characteristics of the physical process under investigation, simulation tools play a crucial role in gaining deeper insights into the physics of under-expanded jets and supporting the development of simplified models for designing and optimizing injection devices. Common methodologies use both explicit (Onorati *et al.* 2022; Buttay *et al.* 2016; Hamzehloo & Aleiferis 2019; Duronio *et al.* 2022) and implicit algorithms (Yosri *et al.* 2020; Rahantamialisoa *et al.* 2022; A & PG 2014). Among these, the use of Large Eddy Simulation (LES) and high-order integration schemes with low numerical dissipation has proven to be particularly effective in replicating the characteristics of under-expanded jets and mixture formation (Hamzehloo & Aleiferis 2014a; Vuorinen *et al.* 2014, 2013).

The literature covers extensive studies on under-expanded jets for gases such as methane, nitrogen, and air (Yu *et al.* 2013a; Banholzer *et al.* 2017; Traxinger *et al.* 2018; Banholzer *et al.* 2019; Xiao *et al.* 2019), with increasing recent interest in hydrogen (Anaclerio *et al.* 2022, 2023; Ballatore & van Oijen 2024; Su *et al.* 2020). Hamzehloo & Aleiferis (2014b, 2016b,a) explored near-nozzle characteristics of various under-expanded jets using a CFD code based on the Advection Upstream Splitting Method (AUSM) discretization for compressible flows, focusing on tip jet penetration, shear layers, and Mach disc structures. In their study, Ren & Wen (2020); Hecht & Panda (2019) examined cryogenic hydrogen ( $H_2$ ) jets using both experimental and numerical methods to assess how the nozzle diameter and pressure ratio affect the structures of jet expansion. The authors utilized a two-dimensional (2D) model with weighted essentially non-oscillatory (WENO) schemes to enhance computational efficiency. A key distinction from typical setups is their use of a total pressure boundary condition instead of a high-pressure reservoir, a method also employed by (Zhang *et al.* 2019a). Further research has examined how real-fluid properties influence jet behaviour. Studies comparing the Redlich-Kwong and Peng-Robinson equations of state revealed that, under certain injection conditions, results differ significantly from those based on the ideal-gas law (Jin & Yao 2021; Rahantamialisoa *et al.* 2023).

However, the most significant limitation of all these studies is the computational resources required. Historically, researchers studied the injection processes relying on Eulerian-Lagrangian CFD codes since they involved liquid fuels. The minimum grid sizing for these investigations is approximately equal to the nozzle diameter (Duronio *et al.* 2025a,b).

Conversely, with gaseous fuels, a correct grid sizing, able to correctly represent the under-expanded jets, is of the order of magnitude of  $D/(30 \div 50)$  (Hamzehloo & Aleiferis 2014a). Such a strict requirement implies a considerable increase in computational resources and severely limits the simulation's feasibility. Careful meshing strategies, like multiple refinement regions and grid size gradually increasing downstream the nozzle exit section (Duronio *et al.* 2022; Hamzehloo & Aleiferis 2016a), can help limit the computational load and allow simulations in acceptable time; nevertheless, increasing the grid dimension degrades the quality of the results, not correctly predicting the air/fuel mixture characteristics, especially when using RANS turbulence models (Wang *et al.* 2024).

Other studies simplify even more the problem by performing 2D simulations (Anaclerio *et al.* 2022; Ren & Wen 2020; Zhang *et al.* 2019a). All these approaches are unreliable for developing new propulsion systems.

The paper reports a CFD investigation of hydrogen under-expanded jets for propulsion applications by high-fidelity GPU-accelerated simulations, adopting high-resolution grid sizing for the jet volume. To this purpose, we adopted AmRex PeleC (Henry de Frahan *et al.* 2024), a high-performance CFD solver for compressible reacting flows that, among the many characteristics, features Adaptive Mesh Refinement (AMR) and high-order order schemes.

We initially validated the simulations by comparison with measurements obtained by Particle Image Velocimetry (PIV) and Schlieren images of under-expanded jets (Ruggles & Ekoto 2012; Edgington-Mitchell *et al.* 2014), then we investigate different injection configurations.

We studied different injection pressure ratios, evaluating the difference in the jet's structure when hydrogen is adopted instead of air and the mixture formation process. We also focus on the nozzle characteristics, showing how the flow drastically changes with annular nozzles and hollow cone jets and how the mixing process is enhanced.

## 2. Mathematical Models and Numerical Method

### 2.1. Mathematical Models

The numerical simulation of the compressible multi-specie flow is performed by the integration of the following governing equations:

$$\left\{ \begin{array}{l} \frac{\partial \rho}{\partial t} + \nabla \cdot (\rho \mathbf{u}) = 0 \\ \frac{\partial (\rho \mathbf{u})}{\partial t} + \nabla \cdot (\rho \mathbf{u} \otimes \mathbf{u}) = -\nabla p + \nabla \cdot \mathbf{\Pi} \\ \frac{\partial (\rho E)}{\partial t} + \nabla \cdot (\rho \mathbf{u} E) = \nabla \cdot (\mathbf{\Pi} \cdot \mathbf{u} - p \mathbf{u}) + \nabla \cdot \mathbf{Q} \\ \frac{\partial (\rho Y_k)}{\partial t} + \nabla \cdot (\rho \mathbf{u} Y_k) = \nabla \cdot \mathcal{F}_k \end{array} \right. \quad (2.1)$$

Here  $\rho, \mathbf{u}, T$ , and  $p$  are the density, velocity, temperature, and pressure, respectively.  $E = e + \mathbf{u} \cdot \mathbf{u}/2$  is the total energy with  $e$  representing the internal energy and  $Y_k$  is the mass fraction of the  $k^{th}$  species. The viscous stress tensor,  $\mathbf{\Pi}$ , under the Newtonian assumption, is given by:

$$\mathbf{\Pi} = \mu [\nabla \mathbf{u} + (\nabla \mathbf{u})^T] + \lambda \mathbf{I} (\nabla \cdot \mathbf{u}) \quad (2.2)$$

where  $\mu$  and  $\lambda$  are viscosity and the Lamè constant, respectively.  $\mathbf{Q}$  is heat flux:

$$\mathbf{Q} = \kappa \nabla T \quad (2.3)$$

where  $\kappa$  is the thermal conductivity.  $\mathcal{F}_k$  is the diffusive transport flux of the  $k$ -th species:

$$\mathcal{F}_k = \rho Y_k D_{k,j} \nabla Y_k \quad (2.4)$$

where  $D_{k,j}$  is the binary diffusivity coefficient between the species.

In all the simulations shown in the paper, we adopted the Dynamic Smagorinsky LES model (Germano *et al.* 1991; Smagorinsky 1963) to accurately resolve the turbulent structures of the jet. For the sake of brevity, we are not reporting full details; the reader is referred to the original papers for a complete description. We supposed Schmidt and Prandtl numbers equal to 0.7 following Vuorinen *et al.* (2014); Hamzehloo & Aleiferis (2019); Duronio *et al.* (2022).

## 2.2. Numerical Method

The numerical integration of the governing equation (2.1) is performed using the solver AmRex PeleC (Henry de Frahan *et al.* 2024), which supports block-structured adaptive mesh refinement (AMR) and GPU parallelization (Zhang *et al.* 2019c). In the code, the inviscid fluxes in (2.1) are discretized using the unsplit piecewise parabolic method (PPM) with hybrid PPM WENO variants (Colella & Woodward 1984; Motheau & Wakefield 2020). The WENO reconstruction is performed with the 7th-order WENO-Z scheme of Balsara & Shu (2000). The diffusion fluxes are discretized in space with second-order centred differences. Temporal integration relies on a standard predictor-corrector approach (Henry de Frahan *et al.* 2024, 2022). Transport coefficients are evaluated from the CHEMKIN transport library and depend on temperature (Kee *et al.* 1986; Ern & Giovangigli 1995). Thermodynamic properties are evaluated by means of the NASA7 polynomial parametrization (McBride 2002).

## 3. Test cases: Characteristics and Numerical Setup

We investigated seven different case studies covering different morphologies of the under-expanded jets. Table 1 reports their main characteristics.

Case N°	Nozzle	Gas/amb	PR	$p_{inj}$ [bar]	$p_{amb}$ [bar]	$T_{amb}$ [K]	$D$ [mm]	Jet cone angle [°]
Validation 1	Round	H <sub>2</sub> /Air	10	9.976	0.9976	292	1.5	N/A
Validation 2	Round	Air/Air	4.2	4.25	1	288	15	N/A
R1	Round	H <sub>2</sub> /Air	4.2	4.25	1	288	15	N/A
R2	Round	H <sub>2</sub> /Air	12.6	12.8	1	288	15	N/A
R3	Round	H <sub>2</sub> /Air	25.2	25.6	1	288	15	N/A
A4	Annular	H <sub>2</sub> /Air	12.6	12.8	1	288	15√2 (*)	90
A5	Annular	H <sub>2</sub> /Air	12.6	12.8	1	288	15√2 (*)	135

Table 1: Test cases details.  $PR$ : pressure ratio;  $p_{inj}$ : injection pressure;  $p_{amb}$ : ambient pressure;  $T_{amb}$ : ambient temperature;  $D$ : nozzle diameter; (\*) : External diameter.

For verification and validation of the simulations, we considered the jets experimentally investigated by Ruggles & Ekoto (2012) and Edgington-Mitchell *et al.* (2014). Both are round jets from circular nozzles. The diameter is equal to 1.5 mm for nozzle 1 and 15 mm for nozzle 2. After these first verification cases, we performed other simulations in which we replicated case 2 by replacing air with hydrogen and then varied the pressure ratio  $PR$  from

4.2 to 25. The last two test cases A4 and A5 deal with annular nozzles, as shown in Figure 1a. We defined them by maintaining the same inner diameter of cases R1-R3 and computing the outer diameter by imposing the same nozzle exit area. These configurations represent hollow cone injectors where the velocity of the gaseous fuel exhibits a radial component ( $\mathbf{u}_r$ ), drastically changing the mixing process with the surrounding air. We studied two different values of the cone angle, representative of real prototypal devices (Montanaro, Alessandro *et al.* 2024).

We implemented the discrete equations on the 3D computational domain reported in figure 1b.

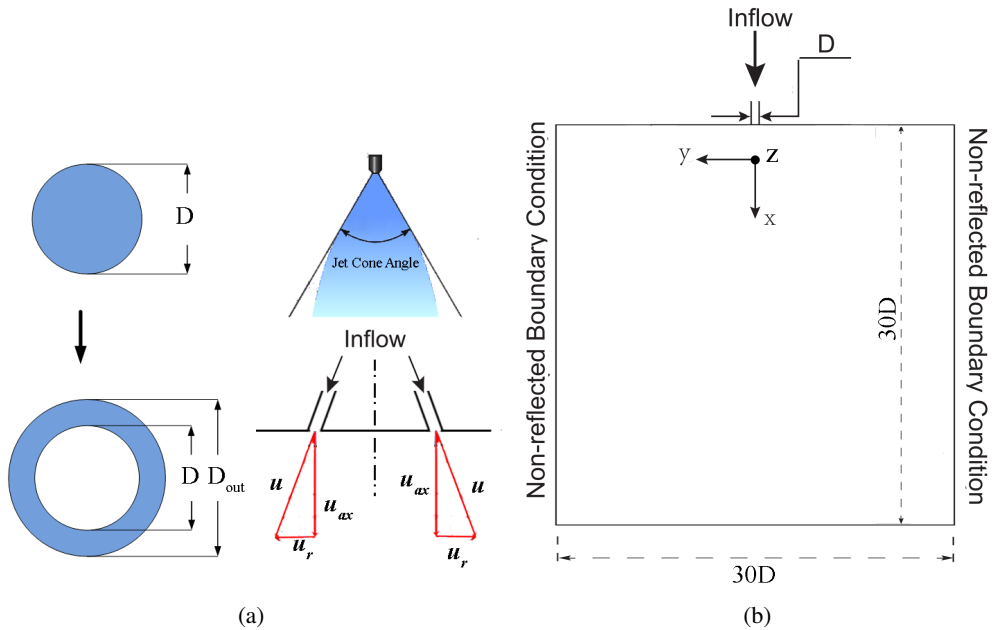


Figure 1: Nozzle configuration investigated and jet cone angle definition Figure 1a.  
Overview of the computational domain Figure 1b

The injection environment is a cubic box with sides equal to  $30D$ . Table 1 summarizes inflow and initial conditions. Validation cases 1 and 2 replicate the test conditions of Ruggles & Ekoto (2012) and Edgington-Mitchell *et al.* (2014). We also imposed open conditions at the bottom boundary while non-reflected boundary conditions at the sides of the box. We refined the mesh using fixed region refinements and Adaptive Mesh Refinement (AMR). In each region, the grid size obeys the law:

$$\Delta_i = \frac{\Delta_b}{2^{R_L}}, \quad (3.1)$$

where  $\Delta_i$  is the dimension of the grid in the generic refinement region,  $\Delta_b$  is the base grid dimension, and  $R_L$  is the refinement level. In all the simulations reported, we used  $R_L = 6$  and  $\Delta_b = D$ ; the size gradually decreases from the maximum to the minimum dimension (placed around the nozzle)  $\Delta_6 = D/64$  with intermediate buffer levels. The region of maximum refinement around the nozzle has size  $8D(\text{jet axis}) \times 3D \times 3D$ .

We activated grid adaptation to guarantee the finest discretization of the whole jet and turned it on when one of the following conditions was verified:

- (i) the velocity magnitude exceeds a threshold value  $V_{thr} = 3.5 \text{ m s}^{-1}$ , i.e.,  $|\mathbf{u}|_{i,j,k} \geq V_{thr}$ ;

(ii) the maximum difference of the density in adjacent locations exceeds a threshold value equal to  $10^{-1} \text{Kg m}^{-3}$ , i.e.

$$\max( \begin{aligned} &|\rho_{i+1,j,k} - \rho_{i,j,k}|, \quad |\rho_{i,j,k} - \rho_{i-1,j,k}|, \\ &|\rho_{i,j+1,k} - \rho_{i,j,k}|, \quad |\rho_{i,j,k} - \rho_{i,j-1,k}|, \\ &|\rho_{i,j,k+1} - \rho_{i,j,k}|, \quad |\rho_{i,j,k} - \rho_{i,j,k-1}| \end{aligned} ) \geq 10^{-1} \text{Kg m}^{-3} \quad (3.2)$$

The integration interval depends on the jet's time-lapse to reach the domain bottom, which is  $O(80 \div 240)D/U_{exit}$ .

Finally, we built two coarser meshes for grid-dependence verification by doubling  $\Delta_b$ .

#### 4. Verification and Validation

We assessed the convergence and uncertainty of the simulations using three grid levels, obtained as described at the end of section 3. We followed the procedure outlined in the classical paper by Roache (1997), in which the procedures now adopted by AIAA, ITTC, and IEEE are described and discussed in detail.

Table 2 reports the average values for the main fields evaluated along the jet's axis and the relative grid convergence index (GCI) based on  $L_2$  norms of the field variations, evaluated in the whole field at the end of the simulations.

	Case 1		Case 2	
	Average Value	GCI	Average Value	GCI
$\rho/\rho_{exit}$	0.25	1.54%	0.47	1.47%
$p/p_{exit}$	0.19	1.27%	0.43	1.27%
$U_x/U_{exit}$	1.10	2.52%	1.17	2.84%

Table 2: Average values on the jet axis and grid convergence index evaluation for validation cases 1 and 2.

To assess the adequacy of the chosen grid for Large Eddy Simulation, we evaluated the modelled kinetic energy and compared it to the total kinetic energy. This evaluation follows the methodology outlined in Di Mascio *et al.* (2022). Figure 2 illustrates the instantaneous ratio between the modelled and total kinetic energy computed once the jet reaches statistically steady conditions on the axial midplane.

The model kinetic energy is significantly lower than the resolved one, and the modeled-to-total kinetic energy ratio is less than 0.2 for most of the domain (the highest values appear in the shear layer). The ratio, therefore, is below the limit of 0.3, which guarantees adequate grid resolution for Large-Eddy Simulation (Pope & Pope 2000).

Next, we compared the numerical results with experimental data. Figure 3 shows the time-averaged shape of the hydrogen jet and the Mach disc recorded using Schlieren imaging by Ruggles & Ekoto (2012) and the numerical results in terms of time-averaged density gradient for validation case 1.

As can be observed, the numerical simulation captures both the morphology of the

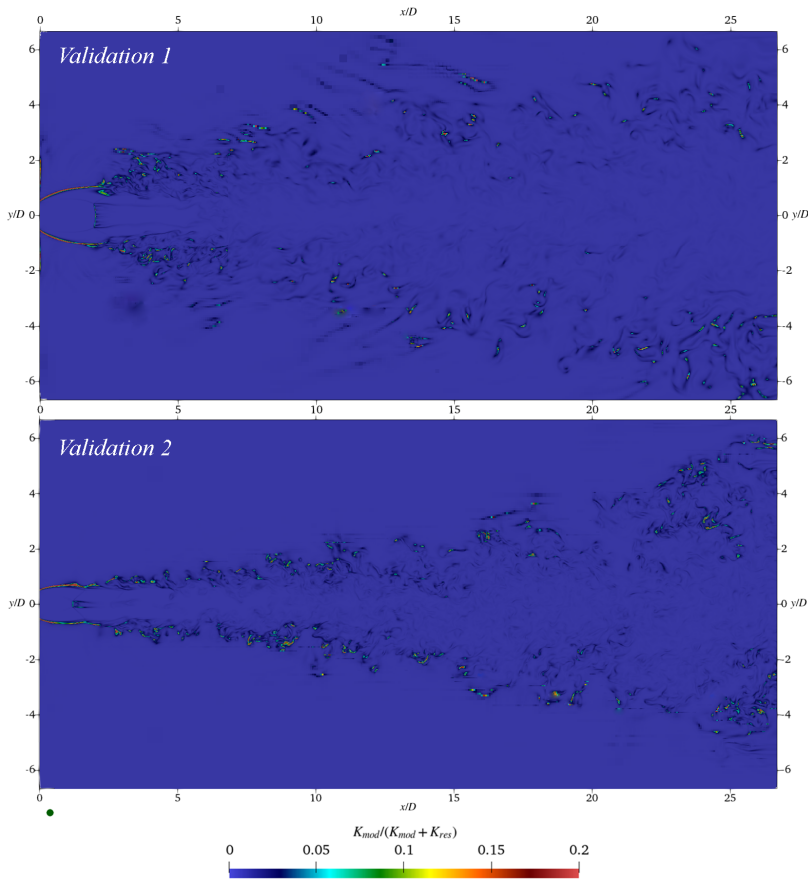


Figure 2:  $K_{mod}/(K_{mod} + K_{res})$  plotted on an axial section of validation cases 1 and 2.

hydrogen jet and the dimensions of the Mach disc. The jet has a peculiar conical shape bounded by a relevant mixing layer. Figure 4 compares the partial derivatives for the density  $\partial\rho/\partial x$  and  $\partial\rho/\partial y$ , relative to validation case 2.

Figure 5 reports the contours of mean axial and transverse flow velocities measured by Edgington-Mitchell *et al.* (2014) and computed in the present paper. We normalized all velocities with the value at the nozzle exit in the hypothesis of sonic conditions at the exit. The simulations correctly reproduce the morphology of the velocity field for both the axial and transverse components. Moreover, the computed Mach disc matches the PIV data, and the magnitude of the velocity is estimated correctly.

Figure 6 compares the time-averaged velocity profiles along the jet axis and several transverse sections. The agreement between the experimental data and the simulation is satisfactory.

## 5. Discussion of the results

We split the discussion into three parts. The first compares H<sub>2</sub> and air under-expanded jets. Then, we investigate the pressure ratio's effects on the hydrogen jets' mixing process with the surrounding air. Finally, we examine the effects of the nozzle design (test cases A4 and A5) by varying the jet angle from 90° to 135°.

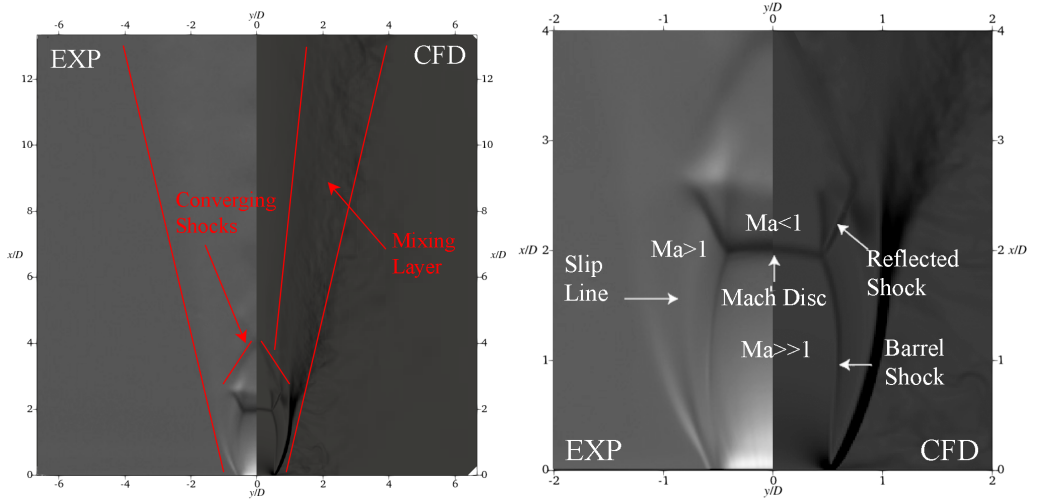


Figure 3: Validation case 1. Comparison of an elaboration of the Schlieren images acquired by Ruggles & Ekoto (2012) and the CFD simulation performed in the current work.

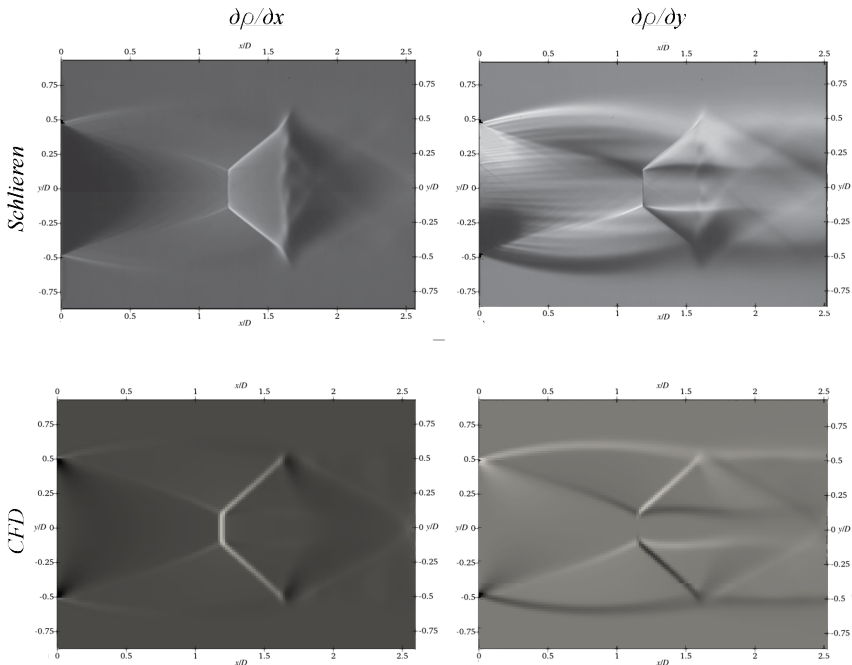


Figure 4: Validation case. Comparison of  $\partial\rho/\partial x$  and  $\partial\rho/\partial y$  from Edgington-Mitchell *et al.* (2014) and the present numerical simulation.

### 5.1. Under-expanded $H_2$ and Air jets

With this section, we aim to investigate the differences in an under-expanded jet's flow structures (and, consequently, mixing characteristics) depending on the chemical species injected. Figure 7 reports the transient evolution of  $\log |\rho/\rho_{amb}|$  for Validation 2 and R1 cases. The conditions for the two test cases are identical, except that hydrogen is injected



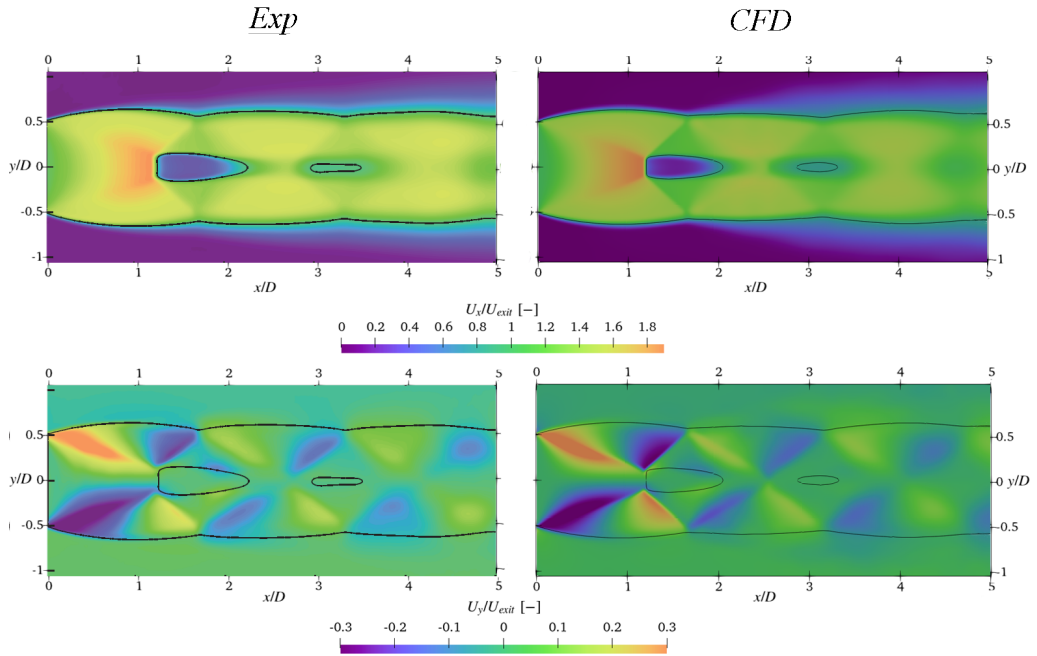


Figure 5: Validation case 2. Comparison of experimental and numerical axial and transverse velocities colormaps.

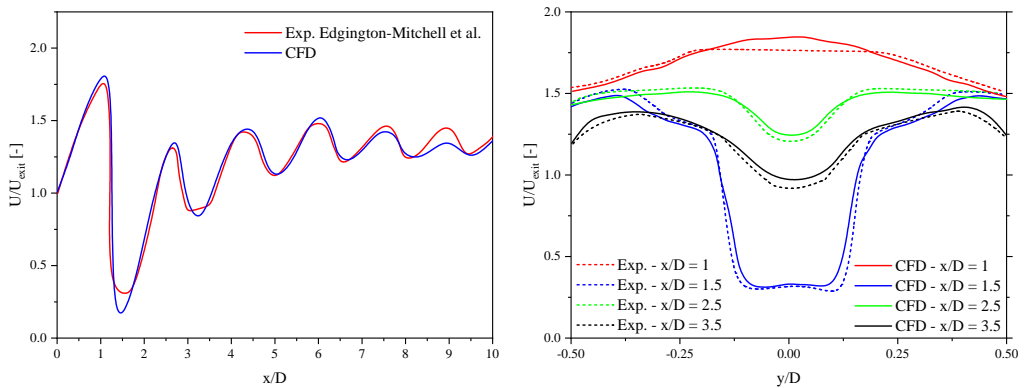


Figure 6: Validation case 2. Time-averaged axial velocity profiles.

instead of air for test R1. In both cases, we observe the classical structures of under-expanded jets, such as barrel shock, cap flow discontinuity, oblique shock waves, slipstream, reflected shocks, and so on (see, e.g., Duronio *et al.* (2022); Zhang *et al.* (2019b)). Nevertheless, we can underline several differences in the flow. First of all, the density of the  $H_2$  jet is lower than the ambient one. This will have a strong influence on the development of the jet. The initial vortex ring entraps much more surrounding fluid in the case of a hydrogen jet than with an air jet. A relevant amount of hydrogen moves aside on the exit section, producing remarkable vortical structures that create a hydrogen-enriched region in the radial direction (a sort of "Coanda effect"). Figure 8 highlights this phenomenon by showing the hydrogen mass fraction in the near nozzle zone for two different time steps. This phenomenon is observed

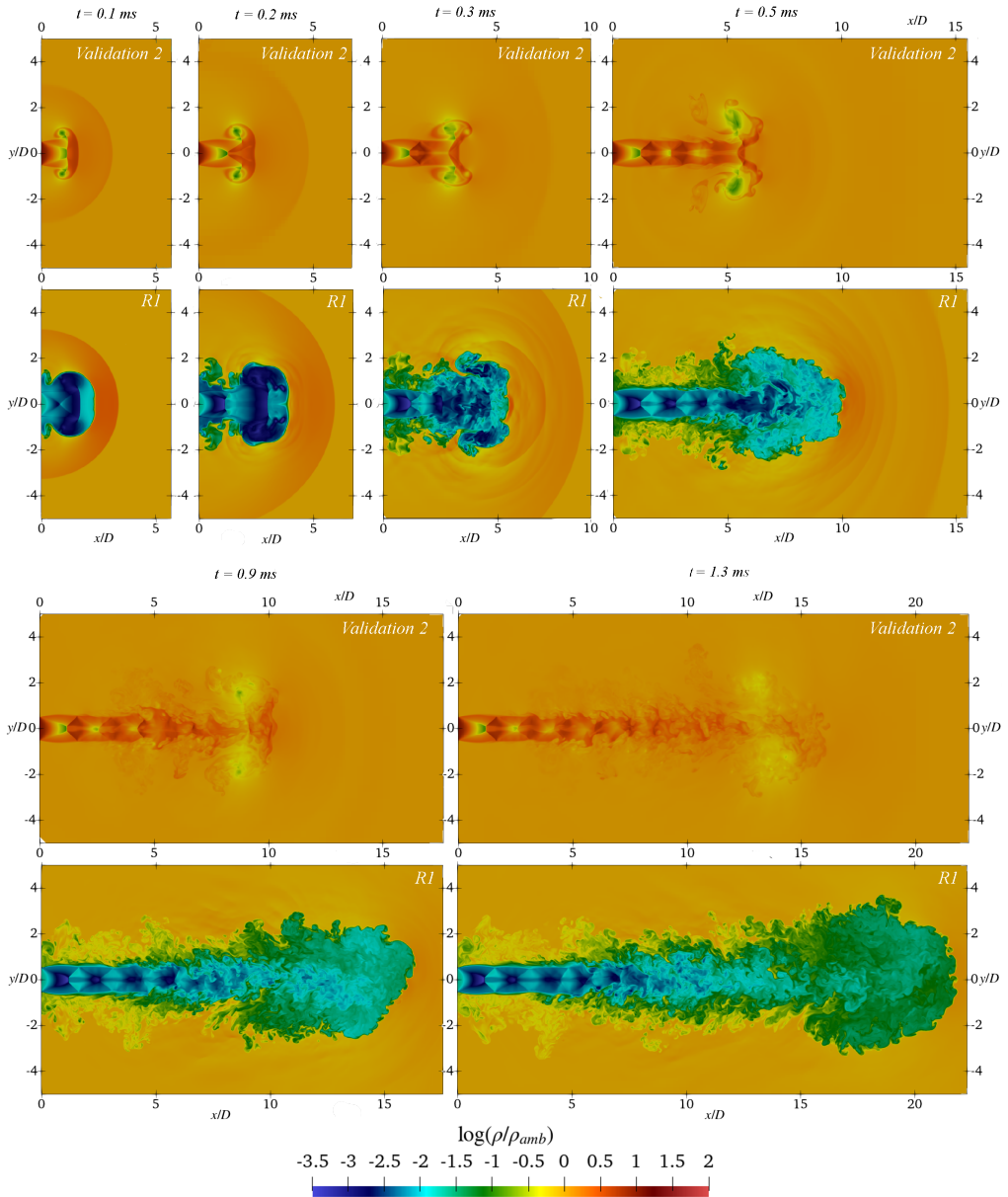


Figure 7: Transient evolution of the jets of the validation case 2 and R1.

only with hydrogen and not air; experimental and CFD studies confirm this behaviour (Leick & Bartole 2023; Merotto *et al.* 2024; Lejsek *et al.* 2024).

As the hydrogen jet evolves, we can observe the development and the evolution of a complex pattern of vortices (see figure 7 at  $t = 0.3 \text{ ms}$  and  $t = 0.5 \text{ ms}$ ), which is absent with air jets, with the presence of a strong shear layer. This complex mixing layer is essential in chemically reactive flow since it promotes interaction with the environmental gas.

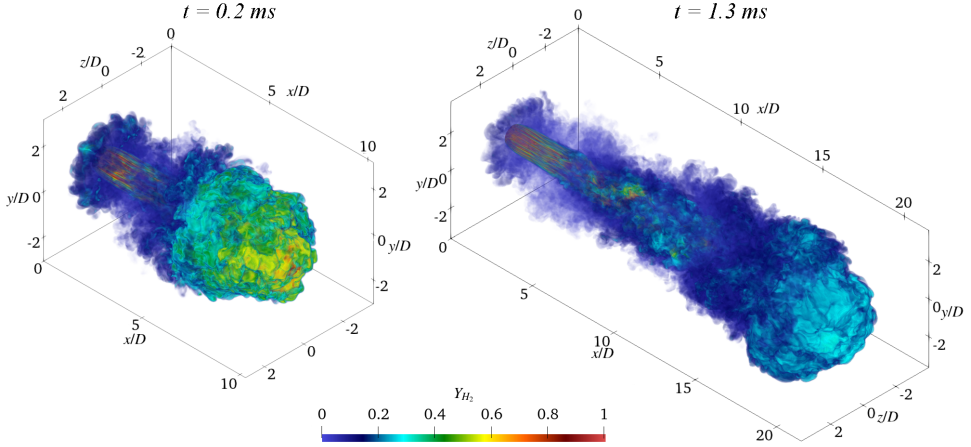
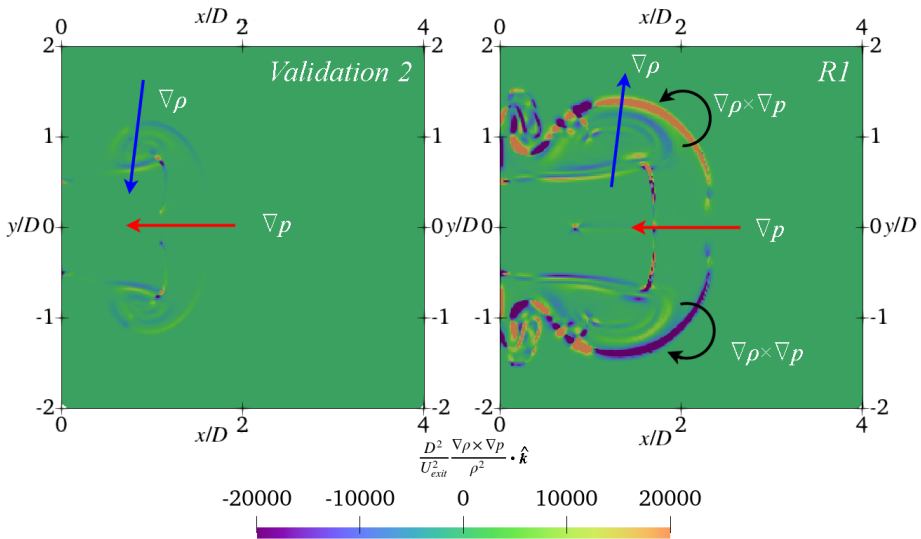


Figure 8: Coanda effect for hydrogen jet.

We can explain the differences between the two jets by examining the vorticity equation

$$\frac{\partial \vec{\omega}}{\partial t} + \vec{u} \cdot \nabla \vec{\omega} = \vec{\omega} \cdot \nabla \vec{u} - \vec{\omega} (\nabla \cdot \vec{u}) + \frac{1}{\rho^2} \nabla \rho \times \nabla p + \nu \nabla^2 \vec{\omega} \quad (5.1)$$

where we have the material of the vorticity on the left-hand side of 5.1, stretching and tilting in the first two terms on the right-hand side, the baroclinic term (the third term on the right), and the diffusion by viscosity in the last term. The baroclinic term produces vorticity when the density gradient is not aligned with the pressure gradient; this term is always present in compressible flows, but we expect strong effects when injecting light gas (hydrogen, in the present simulations) into heavy environment gas with respect to the situation of air-in-air or methane-in-air jets (Duronio & De Vita 2024). Figure 9 reports the  $z$  component of this term in non-dimensional form for the validation case 2 and R1 jets. For the  $H_2$ -in-air jet,

Figure 9: Non-dimensional  $z$  component of the baroclinic term in the vorticity equation on the plane  $z = 0$ . Left: air-in-air jet; right:  $H_2$ -in-air jet

the pressure gradient  $\nabla p$  is almost parallel to the  $x$  axis and directed to the left, while the density gradient is pointing outward with respect to the axis because its core is occupied by hydrogen, as shown by the arrows on the right of figure 9; therefore, the baroclinic term in the vorticity equation induces counterclockwise rotation in the upper part of the figure and clockwise rotation in the lower portion (as shown by the circular arrows in the picture) that push the hydrogen outward. On the contrary, in the air-in-air flow, the density gradient is pointing toward the jet axis, and consequently, the induced rotation is opposite to the one observed with the hydrogen flow. In addition, the magnitude of this term is much lower.

This baroclinic term justifies the completely different morphology of the outer jet between the single-species and the two-species flow. Nonetheless, the shock structure in the core is remarkably similar. Figure 10 is a zoomed view of the Mach disc for the two investigated cases performed after 1.3 ms. The figure shows that the structure of the primary shock cell

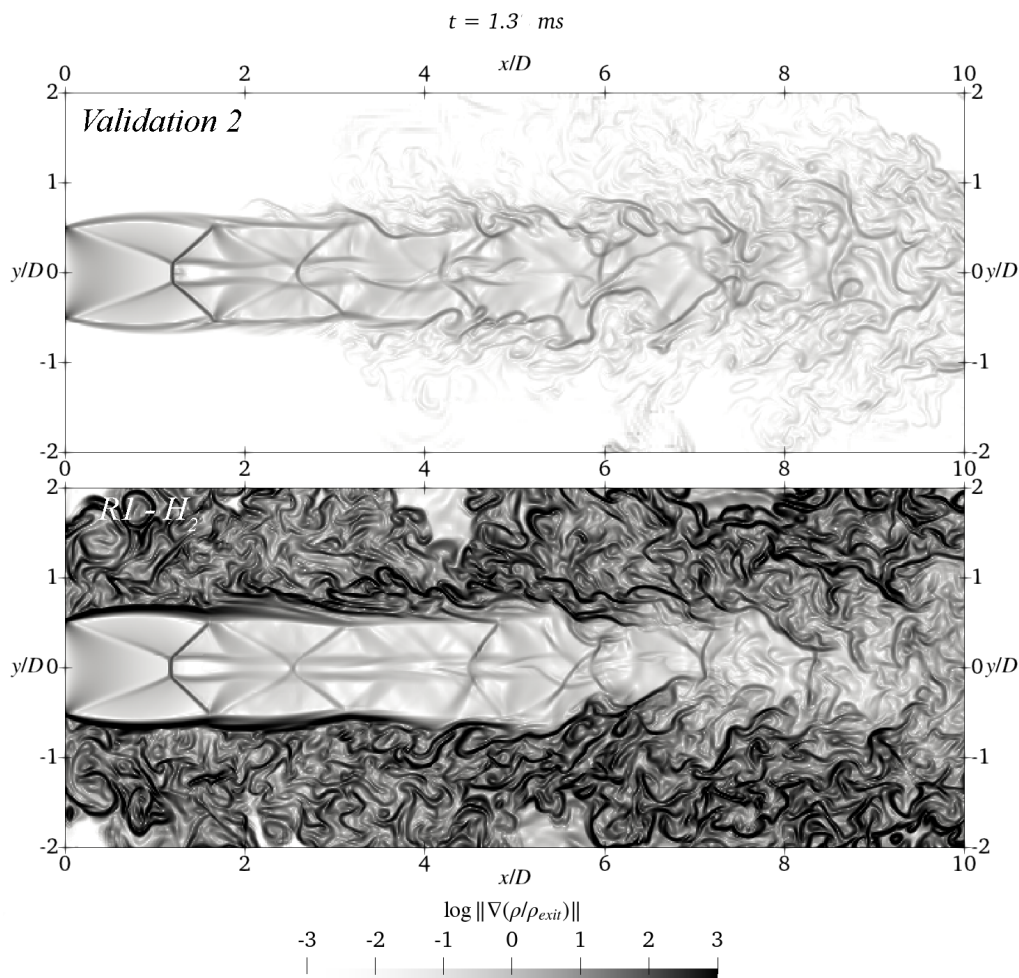


Figure 10: Validation case 2 (top) and R1 (bottom). The logarithm of the non-dimensional density gradient.

is not affected by the species injected, as both the converging shocks and the normal shock have a similar morphology. As previously reported, the two-species jet exhibits a broader

shear layer outside the jet core, where the hydrogen quickly mixes with the surrounding air. To quantify this aspect, we reported in figure 11 the magnitude of the vorticity vector after 1.3 ms. The plot is a volumetric rendering where we removed a quarter of the jet to show its internal structure.

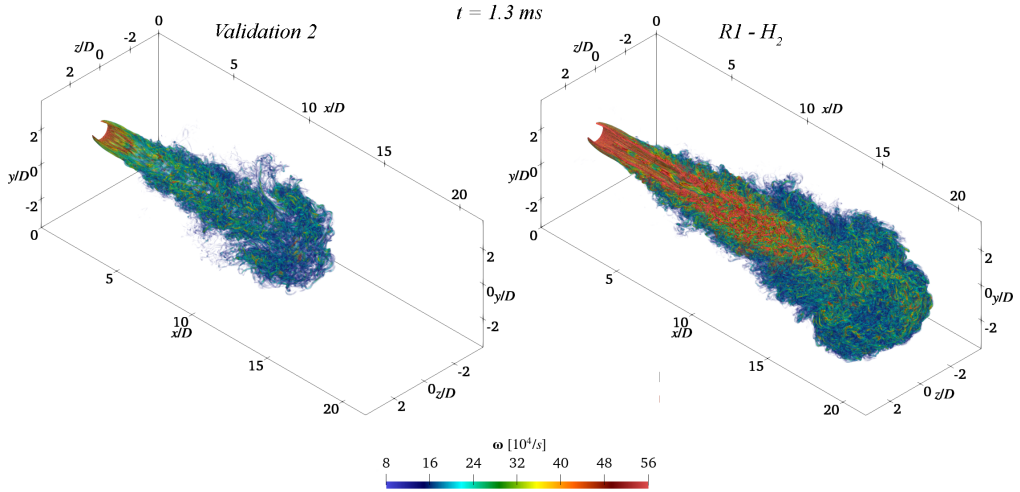


Figure 11: Magnitude of vorticity vector for the air and hydrogen jet with pressure ratio = 4.2.

The vorticity is clearly higher for the hydrogen jet. In the near nozzle zone, both the jets present streamwise vortices outside the potential core with hairpin vortices downstream. As already underlined, these aspects are relevant in chemically reactive flows since the efficiency of the subsequent combustion process strongly depends on the mixing characteristics.

### 5.2. Effects of the pressure ratio on the $H_2$ jets

Figure 12 reports the early stages of the jets R1, R2, and R3 evolution, where the pressure ratio equals 4.2, 12.6, and 25.2, respectively. The early stages of the jets significantly differ when increasing the pressure ratio. The jet with the lower pressure ratio shows two converging shocks that merge at a point located on the jet's axis and a pronounced primary vortex ring. When increasing the upstream pressure, the classical Mach disc shock appears, and the structure of the vortex rings changes. We can observe a primary vortex ring and a significant secondary vortex ring. A cap flow discontinuity delimits a distinguishable zone downstream of the Mach disc shock. The pressure ratio also has a significant effect on the shear layer. Indeed, when looking at the snapshots in figure 12, it can be concluded that a higher injection pressure promotes a broader shear layer, enhances the Coanda effect, and, as discussed below, helps form an ignitable air/fuel mixture. At  $t = 1.2$  ms (figure 13), the final under-expanded structures that characterized the jet can be observed.

Following the classification proposed by Franquet *et al.* (2015) and Duronio *et al.* (2023), the jet of case R1 is highly under-expanded, while the jets R2 and R3 are extremely (or very highly) under-expanded. Indeed, in the first case, the jet has a “barrel” structure that repeats several times downstream. The triple point can be recognized as the intersection of the intercepting shock, the Mach disc, and the reflected shock. Increasing the injection pressure, the structure of the jet is dominated by a single barrel shock. The Mach disc is no longer characterized by a normal shock, but a relevant curvature appears. The lack of a normal shock sequence promotes jet penetration and reduces the so-called potential core's

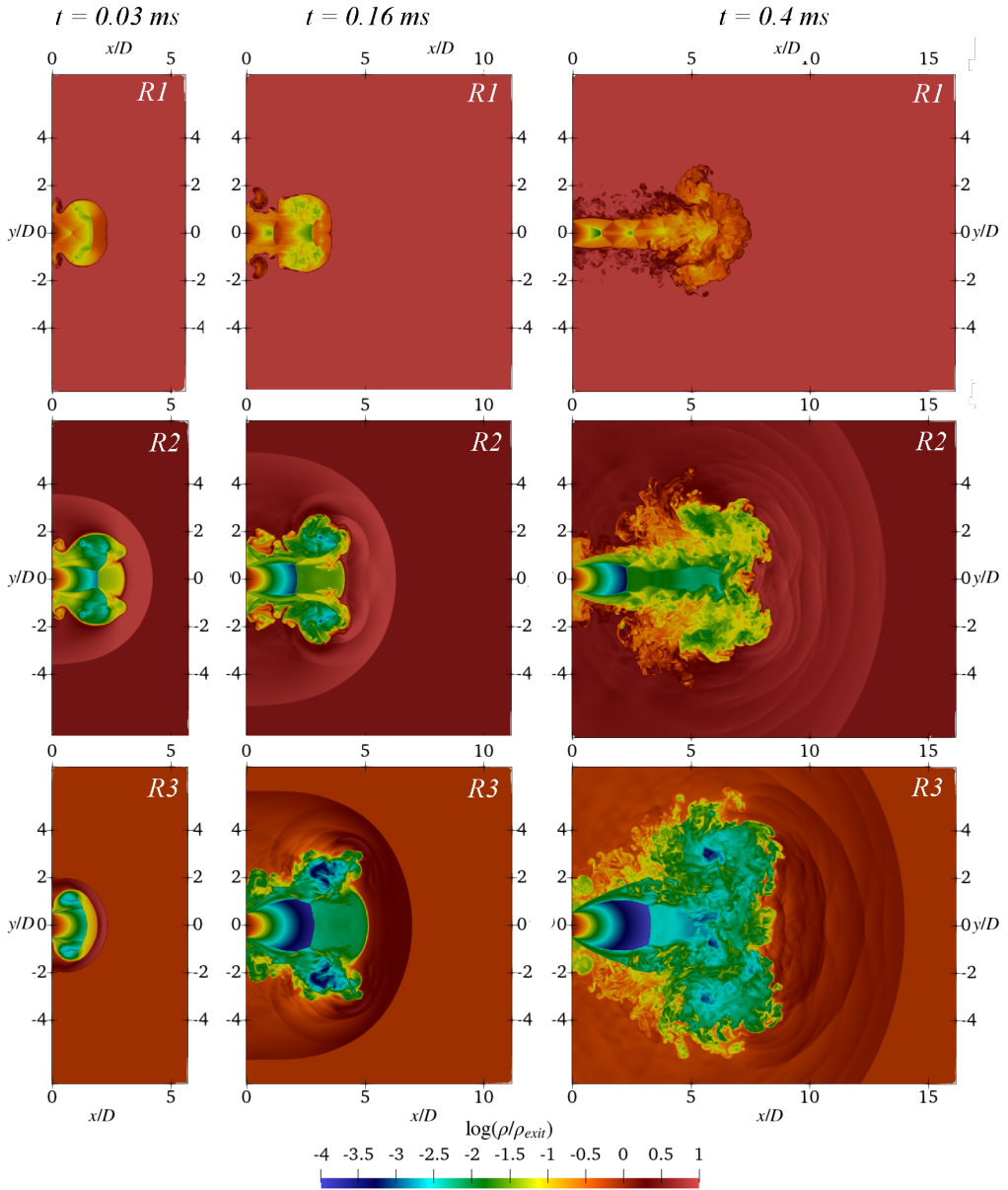


Figure 12: Transient evolution of the hydrogen jets R1, R2, and R3.

length, increasing the mixing between hydrogen and air; this aspect is shown in figure 14, where it can be observed that the zone of the jet characterized by the sequence of barrel shocks does not show any mixing activity, which is completely inhibited. The increase in the pressure ratio reduces the length of this zone.

Figure 15 shows a volumetric rendering of the vorticity magnitude for the three cases. Vorticity is an important parameter in assessing the mixing activity: the higher the pressure ratio, the stronger the vorticity.

Obtaining a quantitative evaluation of the overall quality of the mixture is essential when

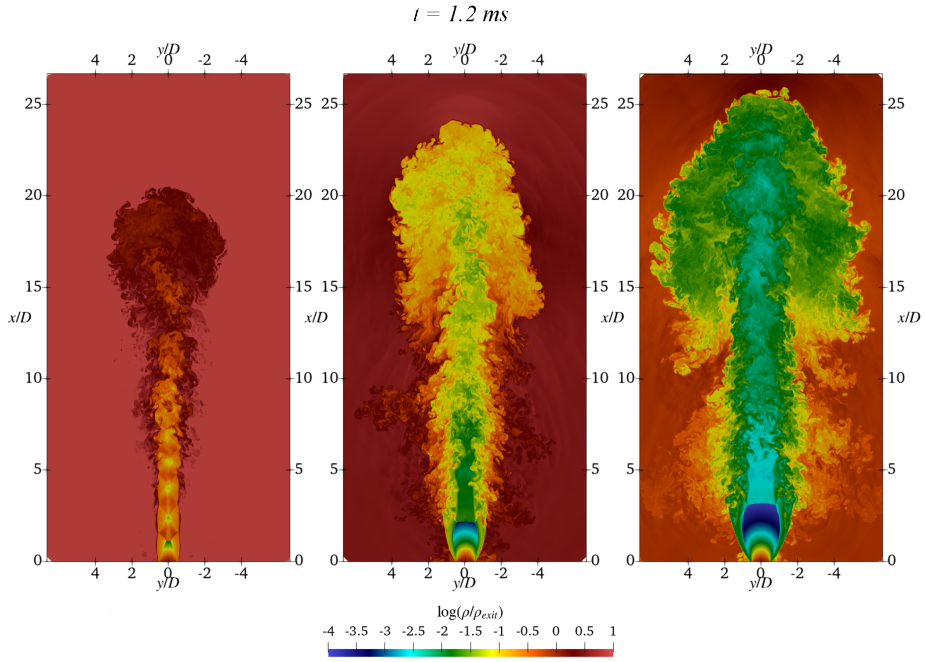


Figure 13: Transient evolution of the hydrogen jets R1, R2, and R3,  $t = 1.2 \text{ ms}$ .

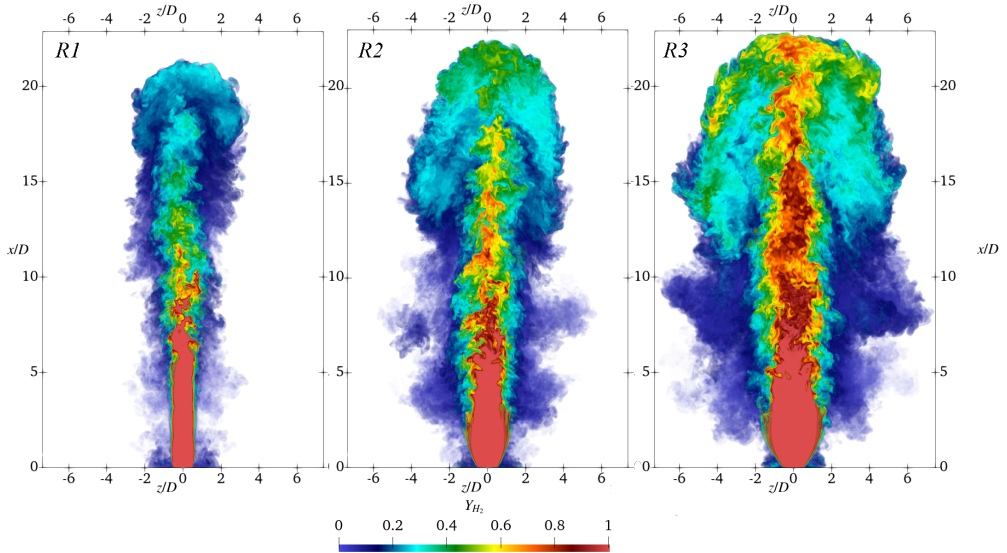


Figure 14: Hydrogen mass fraction for jets R1, R2, and R3,  $t = 1.1 \text{ ms}$ .

dealing with combustion processes. Thus, we defined a discrete mass-weighted probability density function ( $PDF_k(Y_{H_2})$ ) as:

$$PDF_k(Y_{H_2}) = \frac{1}{M_{tot}} \sum_{i=1}^N \begin{cases} \rho_i \delta V_i Y_{H_2,i} & \text{for } k/K \leq Y_{H_2,i} \leq (k+1)/K \\ 0 & \text{otherwise} \end{cases} \quad (5.2)$$

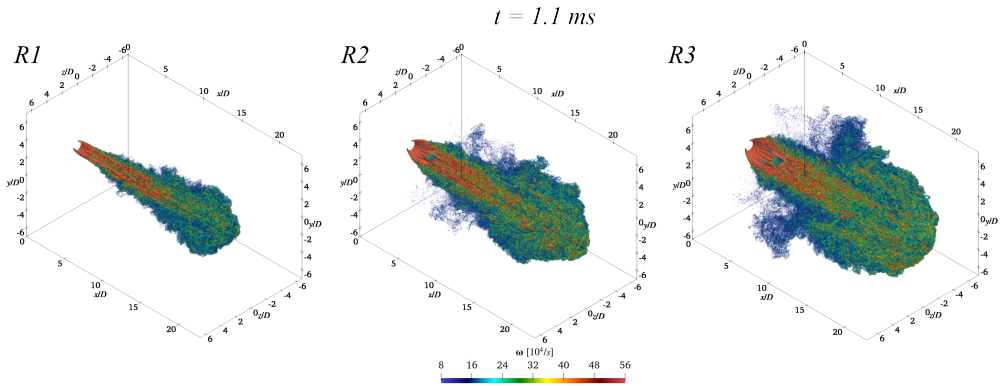


Figure 15: Magnitude of the vorticity vector for cases R1, R2, and R3

where:

- $N$  is the total cell count;
- $K$  is the number of partitions; in this case  $K=100$ ;
- $0 \leq k < 100$
- $PDF_k(\cdot)$  is the probability density function;
- $\delta V_i$  is the cell volume;
- $\rho_i$  is the mixture density;
- $Y_{H_2,i}$  is the hydrogen mass fraction in the  $i$ -th cell;
- $M_{tot}$  is the total injected mass at a certain instant;

Figure 16 reports the probability density function distribution and the mass injected for the three cases investigated at 1.2 ms.

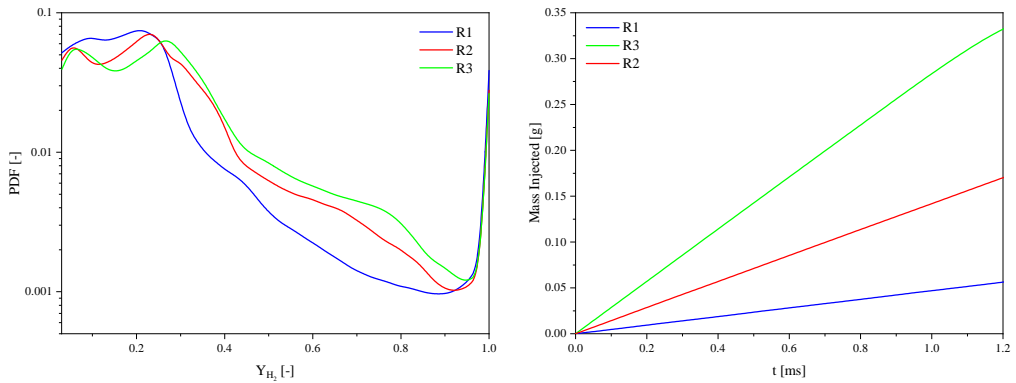


Figure 16: Probability distribution of  $H_2$  mass fraction at 1.2 ms and hydrogen mass injected in dimensional terms.

The PDFs for the three cases are very similar, showing a peak around  $Y_{H_2} = 0.3$ ; of course, the amount of hydrogen mass injected grows with the injection pressure.

### 5.3. Effects of the nozzle shape

The nozzle design for gaseous injectors is essential to developing efficient injection devices. For this reason, we investigate two annular nozzles characterized by jet angles equal to  $90^\circ$  (case A4) and  $135^\circ$  (case A5). Figure 17 compares the jet's transient evolution for the early



stages of the simulated transient. As before, we plotted the  $\log(\rho/\rho_{exit})$ . The evolution is

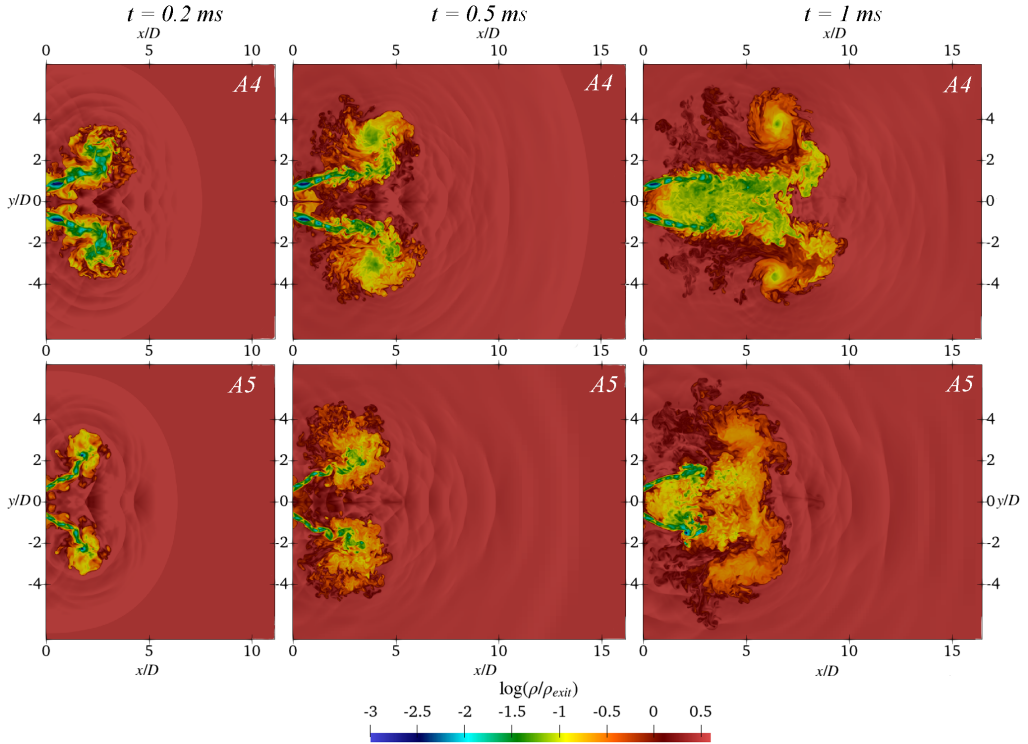


Figure 17: Early stages of the transient evolution for the jets A4 and A5. Plot of the logarithm of the non-dimensional density gradient.

very different when compared with the round jet. At  $t = 0.2 \div 0.5$  ms, the hollow-cone jets present a conical structure characterized by the angle imposed. The pressure inside the cone becomes gradually lower than the external one, and the jet continues its evolution by contracting towards the  $x$ -axis, as shown in figure 18 where we reported the time-averaged velocity vectors and the pressure field over  $0 \leq t \leq 2.4$  ms on the axial plane.

Outside the core, in the near nozzle zone, air cannot enter within the jet due to the presence of a series of shock cells. On the other hand, we can observe a series of vortices rotating toward the central axis that drags the hydrogen into the jet's core. This flow path extends for approximately  $4D$  downstream of the nozzle exit section. The intensity of this phenomenon increases with the jet cone angle. As illustrated by figure 19, this circulation remains active until the jet spreads in the surroundings. The subsequent injection stages are characterized by the jet advancing toward the right boundary of the domain with a velocity greater for jet A4 because of the smaller cone angle. Although the shape of the jet is similar, the cone angle modifies the hydrogen concentration, as shown in the figure by  $\log(\rho/\rho_{exit})$ . Various experimental investigations confirm this evolution mechanism, and it is characteristic of hollow cone jets Lee *et al.* (2021); Coratella *et al.* (2024); Montanaro, Alessandro *et al.* (2024).

Figure 20 shows the Mach number for the two jets at  $t = 2.4$  ms.

The hollow conical structure of the jet determines a ring-shaped spatial arrangement of the shock waves. The single Mach disc observed with the circular nozzle disappears, but barrel shocks can also be recognized for test cases in A4 and A5; moreover, their size diminishes

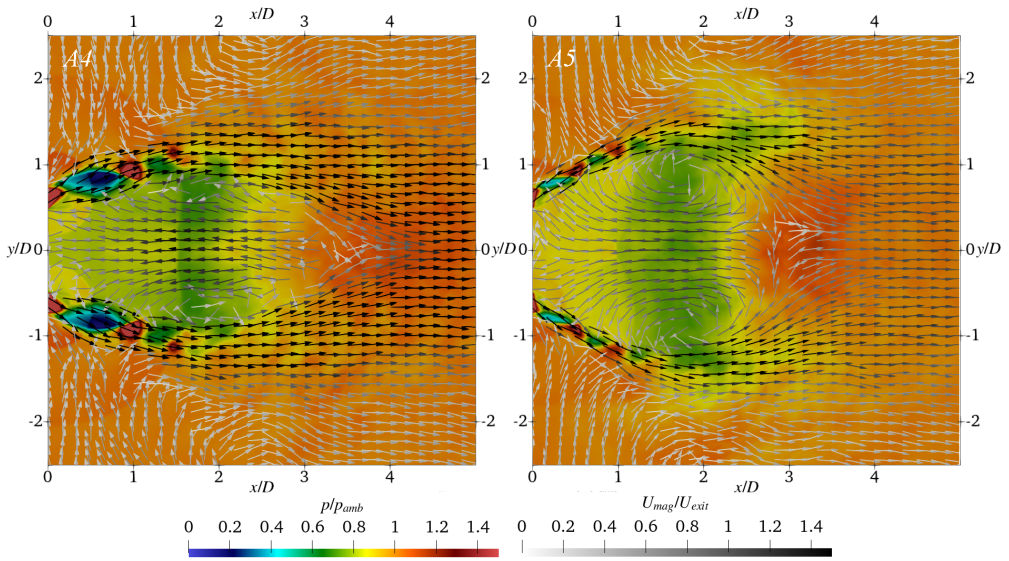


Figure 18: Time averaged pressure field and velocity vectors.

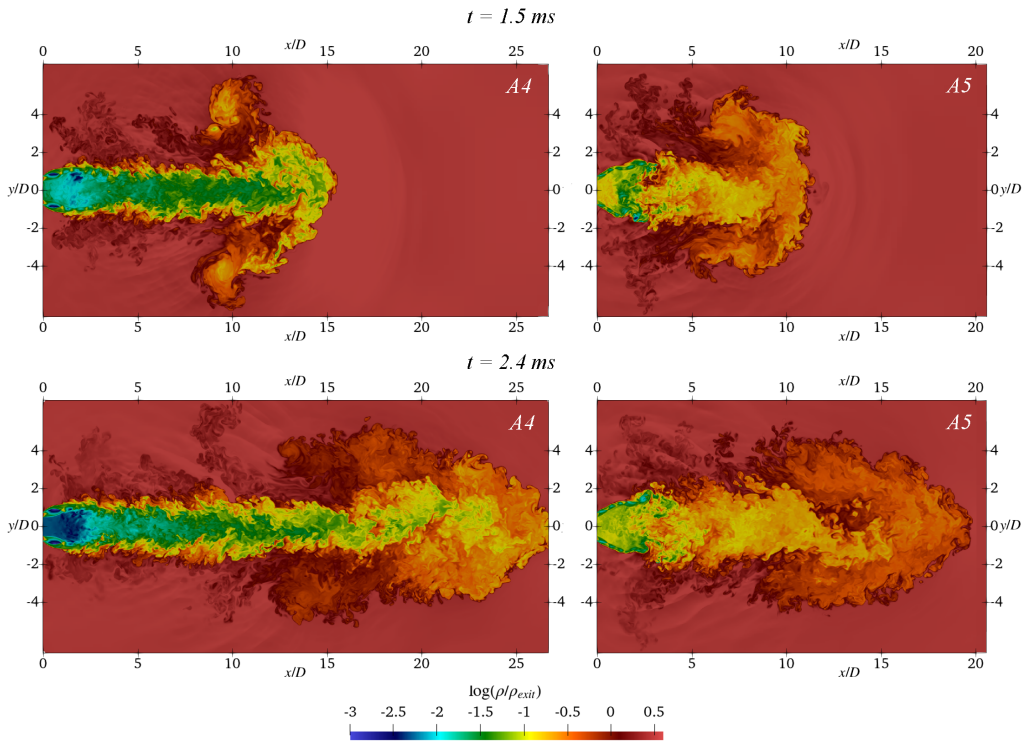


Figure 19: Transient evolution of the jets A4 and A5. Late stages.

with the increasing jet angle. The number of these shock cells is larger for case A5. We can conclude that, when performing a hollow cone injection, the increase of the jet angle

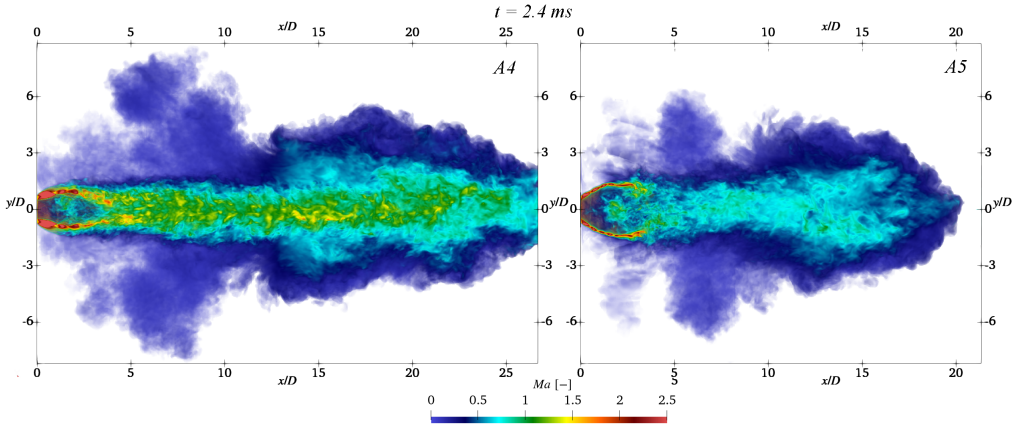


Figure 20: Mach number plot for cases A4 and A5,  $t = 2.4$  ms.

reduces the Mach number and the hydrogen velocity; therefore, with the same nozzle area, the injection of the same amount of  $H_2$  requires a longer time.

To quantitatively assess the mixture quality obtainable with a hollow cone injection, in figure 21 we plotted the PDF and the average  $H_2$  concentration into the domain as a function of time for the cases R2, A4, and A5. To have comparable results, we plotted the PDF at the time instant required to have an injected non-dimensional mass equal to 100 for all cases.

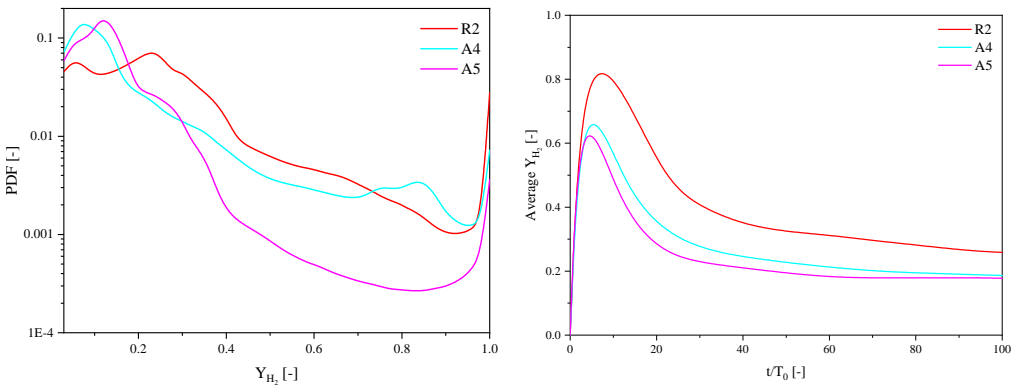


Figure 21: Probability distribution of  $H_2$  mass fraction and average  $H_2$  mass fraction as a function of time.

The improvement obtainable with the hollow-cone configurations, particularly with the one in test case A5, is remarkable. In the latter configuration, the high-concentration areas where the hydrogen is not flammable are almost entirely removed, and the average concentration decreases significantly. This is confirmed by figure 22, where we reported the hydrogen mass fraction at the time instant when the injected mass is the same.

The increased jet angle promotes the mixing with the surrounding air and almost completely removes the hydrogen-rich potential core. It can be seen that the region where the hydrogen mass fraction is close to one is shrunk, for case A5, to a hollow cone around the annular inflow section.

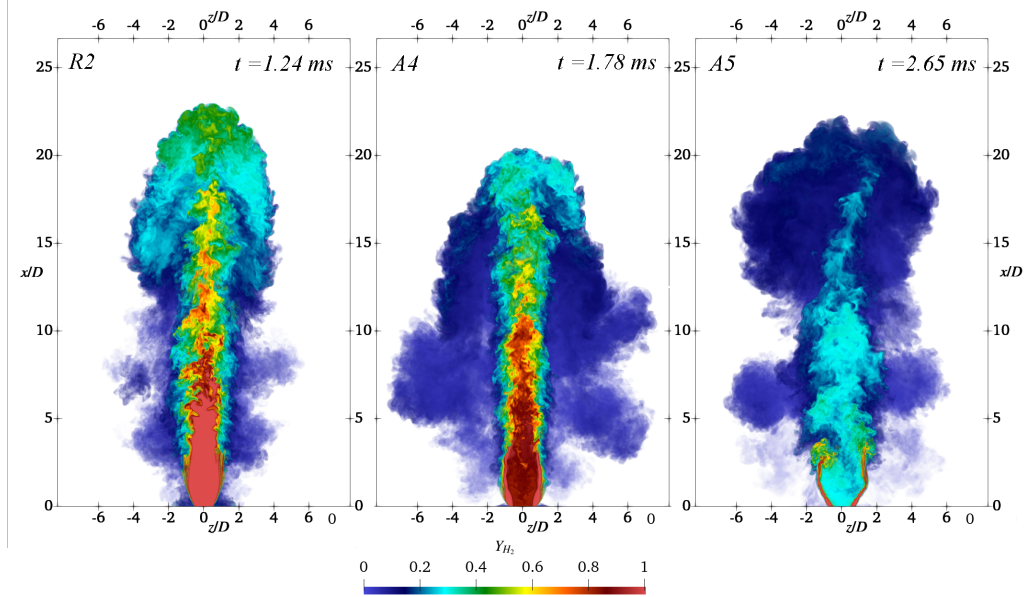


Figure 22: Hydrogen mass fraction for the jets R2, A4 and, A5. Time is relative to a non-dimensional mass equal to 100 injected in the computational domain.

## 6. Conclusions

We investigated hydrogen under-expanded jets using Large Eddy Simulations of round and annular nozzles. We focused on the jet's characteristics and, more importantly, the mixture formation process.

The simulations were verified and validated against experimental particle image velocimetry and Schlieren images when available. The simulated jets, the Mach disc dimensions, and the resulting velocity field closely align with experimental observations.

The analysis covers injection pressure ratios from 4.2 to 25.6 and examines the nozzle geometrical configuration's effects on the air-fuel mixture's characteristics. The main outcomes are:

- The transient evolution of hydrogen under-expanded jets radically differs from the one observed for air. In particular, the mixing outside the jet core is enhanced by the baroclinic effect. On the contrary, the structure of the jet core is similar for the two flows in terms of shock structures.
- The physical characteristics of the hydrogen trigger an intense interaction with the surrounding air. The hydrogen jet develops very high vorticity and engulfs a large air volume.
- The pressure ratio is a key parameter in controlling the jet's characteristics. It can be used to inject the proper amount of fuel in a reduced time.
- Increasing the pressure ratio, the repeated shock cells disappear, and we have a unique Mach disc. Besides, the potential core becomes smaller for higher pressure ratios. As the potential core is the zone of the jet where there is no mixing activity when reducing it, the mixture quality improves.
- Hollow cone jets have a drastically different morphology when compared to the classical round jets. Ring-shaped shock cells substitute the Mach disc, and the jet from highly under-expanded becomes weakly under-expanded. The Mach number decreases, and injecting the same amount of hydrogen requires a longer time.
- The recirculation zone developing downstream the nozzle for approximately 4D sig-

nificantly enhances the mixing activity, removes the hydrogen-rich core and gives a higher quality mixture.

– A jet cone angle greater than  $90^\circ$  improves the mixture quality from the combustion point of view. With a jet cone angle equal to  $135^\circ$  we manage to quickly reduce the average hydrogen concentration already in the first phase of the injection and to remove the zones where the hydrogen concentration exceeds 0.4 completely.

## Acknowledgment

This work has been funded by the European Union - NextGenerationEU, Mission 4, Component 1, under the Italian Ministry of University and Research (MUR) National Innovation Ecosystem grant ECS00000041 - VITALITY - CUP E13C22001060006.

## Declaration of Interests

The authors report no conflict of interest.

## REFERENCES

- A, HAMZEHLOO & PG, ALEIFERIS 2014 Large eddy simulation of near-nozzle shock structure and mixing characteristics of hydrogen jets for direct-injection spark-ignition engines .
- ALLOCCA, LUIGI, MONTANARO, ALESSANDRO, MECCARIELLO, GIOVANNI, DURONIO, FRANCESCO, RANIERI, STEFANO & DE VITA, ANGELO 2020 Under-Expanded Gaseous Jets Characterization for Application in Direct Injection Engines: Experimental and Numerical Approach. *SAE Technical Papers* **2020-April** (April), 1–15.
- ANACLERIO, GIUSEPPE, CAPURSO, TOMMASO & TORRESI, MARCO 2023 Gas-dynamic and mixing analysis of under-expanded hydrogen jets: effect of the cross section shape. *Journal of Fluid Mechanics* **970**, A8.
- ANACLERIO, GIUSEPPE, CAPURSO, TOMMASO, TORRESI, MARCO & CAMPOREALE, SERGIO MARIO 2022 Numerical characterization of hydrogen under-expanded jets: Influence of the nozzle cross-section shape. , vol. 2385. Institute of Physics.
- BALLATORE, A. & VAN OIJEN, J.A. 2024 Pressure-based large-eddy simulation of under-expanded hydrogen jets for engine applications. *International Journal of Hydrogen Energy* **49**, 771–783.
- BALSARA, DINSHAW S. & SHU, CHI-WANG 2000 Monotonicity preserving weighted essentially non-oscillatory schemes with increasingly high order of accuracy. *Journal of Computational Physics* **160** (2), 405–452.
- BANHOLZER, MATTHIAS, MÜLLER, HAGEN & PFITZNER, MICHAEL 2017 Numerical investigation of the flow structure of underexpanded jets in quiescent air using real-gas thermodynamics. American Institute of Aeronautics and Astronautics Inc, AIAA.
- BANHOLZER, M., VERA-TUDELA, W., TRAXINGER, C., PFITZNER, M., WRIGHT, Y. & BOULOUCHOS, K. 2019 Numerical investigation of the flow characteristics of underexpanded methane jets. *Physics of Fluids* **31** (5), 056105.
- BARTOLUCCI, L., CORDINER, S., MULONE, V., SCARCELLI, R., WALLNER, T., SWANTEK, A.B., POWELL, C.F. & KASTENGREN, A.L. 2020 Gaseous jet through an outward opening injector: Details of mixing characteristic and turbulence scales. *International Journal of Heat and Fluid Flow* **85**, 108660.
- BUTTAY, R., LEHNASCH, G. & MURA, A. 2016 Analysis of small-scale scalar mixing processes in highly under-expanded jets. *Shock Waves* **26**, 193–212.
- CARCANO, S., BONAVENTURA, L., ESPOSTI ONGARO, T. & NERI, A. 2013 A semi-implicit, second-order-accurate numerical model for multiphase underexpanded volcanic jets. *Geoscientific Model Development* **6** (6), 1905–1924.
- COLELLA, PHILLIP & WOODWARD, PAUL R 1984 The piecewise parabolic method (ppm) for gas-dynamical simulations. *Journal of Computational Physics* **54** (1), 174–201.
- CORATELLA, C., TINCHON, A., OUNG, R., DORADOUX, L. & FOUCHER, F. 2024 Experimental investigation of the combined impact of backpressure with the pintle dynamic on the hydrogen spray exiting a medium pressure di outward-opening injector. *International Journal of Hydrogen Energy* **49**, 432–449.

- DI MASCIÒ, A., DUBBIOSO, G. & MUSCARI, R. 2022 Vortex structures in the wake of a marine propeller operating close to a free surface. *Journal of Fluid Mechanics* **949**, A33.
- DONG, QUAN, LI, YUE, SONG, ENZHE, FAN, LIYUN, YAO, CHONG & SUN, JUN 2018 Visualization research on injection characteristics of high-pressure gas jets for natural gas engine. *Applied Thermal Engineering* **132**, 165–173.
- DURONIO, FRANCESCO & DE VITA, ANGELO 2024 Cfd analysis of hydrogen and methane turbulent transitional under-expanded jets. *International Journal of Heat and Fluid Flow* **107**, 109381.
- DURONIO, FRANCESCO, LIEN, HAO-PIN & DE VITA, ANGELO 2025a Cfd unified approach under eulerian–lagrangian framework for methanol and gasoline direct injection sprays in evaporative and flash boiling conditions. *International Journal of Multiphase Flow* **182**, 105048.
- DURONIO, FRANCESCO, MONTANARO, ALESSANDRO, ALLOCCA, LUIGI, RANIERI, STEFANO & DE VITA, ANGELO 2022 Effects of thermodynamic conditions and nozzle geometry in gaseous fuels direct injection process for advanced propulsion systems. In *WCX SAE World Congress Experience*. SAE International.
- DURONIO, FRANCESCO, RANIERI, STEFANO, MASCIÒ, ANDREA DI & VITA, ANGELO DE 2021 Simulation of high pressure, direct injection processes of gaseous fuels by a density-based openfoam solver. *Physics of Fluids* **33** (6), 066104.
- DURONIO, FRANCESCO, VILLANTE, CARLO & DE VITA, ANGELO 2023 Under-expanded jets in advanced propulsion systems: A review of latest theoretical and experimental research activities. *Energies* **16** (18).
- DURONIO, FRANCESCO, ZHANG, ANQI, ZHAO, LE & DE VITA, ANGELO 2025b Assessment of an effervescent breakup model for lagrangian simulations of real fuel sprays. *International Journal of Thermofluids* **25**, 100991.
- EDGINGTON-MITCHELL, DANIEL, HONNERY, DAMON R. & SORIA, JULIO 2014 The underexpanded jet Mach disk and its associated shear layer. *Physics of Fluids* **26** (9), 096101.
- ERN, ALEXANDRE & GIOVANGIGLI, VINCENT 1995 Fast and accurate multicomponent transport property evaluation. *Journal of Computational Physics* **120** (1), 105–116.
- FOX, JOHN H. 1974 On the structure of jet plumes. *AIAA Journal* **12** (1), 105–107.
- FRANQUET, ERWIN, PERRIER, VINCENT, GIBOUT, STÉPHANE & BRUEL, PASCAL 2015 Free underexpanded jets in a quiescent medium: A review. *Progress in Aerospace Sciences* **77**, 25–53.
- GERMANO, MASSIMO, PIOMELLI, UGO, MOIN, PARVIZ & CABOT, WILLIAM H. 1991 A dynamic subgrid-scale eddy viscosity model. *Physics of Fluids A: Fluid Dynamics* **3** (7), 1760–1765, arXiv: [https://pubs.aip.org/aip/pof/article-pdf/3/7/1760/12459782/1760\\_1\\_online.pdf](https://pubs.aip.org/aip/pof/article-pdf/3/7/1760/12459782/1760_1_online.pdf).
- HAMZEHLOO, A. & ALEIFERIS, P.G. 2014a Large eddy simulation of highly turbulent under-expanded hydrogen and methane jets for gaseous-fuelled internal combustion engines. *International Journal of Hydrogen Energy* **39** (36), 21275–21296.
- HAMZEHLOO, A. & ALEIFERIS, P. G. 2014b Large eddy simulation of highly turbulent under-expanded hydrogen and methane jets for gaseous-fuelled internal combustion engines. *International Journal of Hydrogen Energy* **39**, 21275–21296.
- HAMZEHLOO, A. & ALEIFERIS, P. G. 2016a Gas dynamics and flow characteristics of highly turbulent under-expanded hydrogen and methane jets under various nozzle pressure ratios and ambient pressures. *International Journal of Hydrogen Energy* **41**, 6544–6566.
- HAMZEHLOO, A. & ALEIFERIS, P. G. 2016b Numerical modelling of transient under-expanded jets under different ambient thermodynamic conditions with adaptive mesh refinement. *International Journal of Heat and Fluid Flow* **61**, 711–729.
- HAMZEHLOO, ARASH & ALEIFERIS, PAVLOS G. 2019 LES and RANS modelling of under-expanded jets with application to gaseous fuel direct injection for advanced propulsion systems. *International Journal of Heat and Fluid Flow* **76** (January), 309–334.
- HECHT, ETHAN S. & PANDA, PRATIKASH P. 2019 Mixing and warming of cryogenic hydrogen releases. *International Journal of Hydrogen Energy* **44** (17), 8960–8970, special issue on The 7th International Conference on Hydrogen Safety (ICHS 2017), 11–13 September 2017, Hamburg, Germany.
- HENRY DE FRAHAN, MARC T., ESCLAPEZ, LUCAS, ROOD, JON, WIMER, NICHOLAS T., MULLOWNEY, PAUL, PERRY, BRUCE A., OWEN, LONDON, SITARAMAN, HARISWARAN, YELLAPANTULA, SHASHANK, HASSANALY, MALIK, RAHIMI, MOHAMMAD J., MARTIN, MICHAEL J., DORONINA, OLGA A., A., SREEJITH N., RIETH, MARTIN, GE, WENJUN, SANKARAN, RAMANAN, ALMGREN, ANN S., ZHANG, WEIQUN, BELL, JOHN B., GROUT, RAY, DAY, MARC S. & CHEN, JACQUELINE H. 2024 The pele simulation suite for reacting flows at exascale. *Proceedings of the 2024*

- SIAM Conference on Parallel Processing for Scientific Computing* pp. 13–25, arXiv: <https://epubs.siam.org/doi/pdf/10.1137/1.9781611977967.2>.
- HENRY DE FRAHAN, MARC T, ROOD, JON S, DAY, MARC S, SITARAMAN, HARISWARAN, YELLAPANTULA, SHASHANK, PERRY, BRUCE A, GROUT, RAY W, ALMGREN, ANN, ZHANG, WEIQUN, BELL, JOHN B & CHEN, JACQUELINE H 2022 PeleC: An adaptive mesh refinement solver for compressible reacting flows. *The International Journal of High Performance Computing Applications* **37** (2), 115–131.
- JIN, YICHAO & YAO, WEI 2021 Les investigation of real-fluid effect on underexpanded jets. American Institute of Aeronautics and Astronautics Inc, AIAA.
- KEE, ROBERT J, DIXON-LEWIS, GRAHAM, WARNATZ, JÜRGEN, COLTRIN, MICHAEL E & MILLER, JAMES A 1986 A fortran computer code package for the evaluation of gas-phase multicomponent transport properties. *Sandia National Laboratories Report SAND86-8246* **13**, 80401–1887.
- LEE, SANGUK, KIM, GYEONGGON & BAE, CHOONGSIK 2021 Behavior of hydrogen hollow-cone spray depending on the ambient pressure. *International Journal of Hydrogen Energy* **46** (5), 4538–4554.
- LEICK, PHILIPPE & BARTOLE, KEVIN 2023 Experimental investigation into the shift of gdi sprays towards nearby walls via the coandă effect using detailed shadow imaging, particle and structure image velocimetry. *Experiments in Fluids* **64**, 144.
- LEJSEK, DAVID, SEBOLDT, DIMITRI, LEICK, PHILIPPE, GRZESZIK, ROMAN, FRANK, MICHAEL & STAPE, KARL GEORG 2024 Experimental toolchain for evaluation of mixture formation and combustion in hydrogen engines for light duty applications. In *2024 Stuttgart International Symposium on Automotive and Engine Technology* (ed. André Casal Kulzer, Hans-Christian Reuss & Andreas Wagner), pp. 102–129. Wiesbaden: Springer Fachmedien Wiesbaden.
- VON DER LINDEN, JENS, KIMBLIN, CLARE, MCKENNA, IAN, BAGLEY, SKYLER, LI, HSIAO-CHI, HOUIM, RYAN, KUENY, CHRISTOPHER S, KUHL, ALLEN, GROTE, DAVE, CONVERSE, MARK, VOSSEN, CARON E J, STERN, SÖNKE, CIMARELLI, CORRADO & SEARS, JASON 2021 Standing shock prevents propagation of sparks in supersonic explosive flows. *Communications Earth & Environment* **2**, 195.
- MCBRIDE, BONNIE J 2002 *NASA Glenn coefficients for calculating thermodynamic properties of individual species*. National Aeronautics and Space Administration, John H. Glenn Research Center . . .
- MEROTTO, L., BALMELLI, M. & SOLTIC, P. 2024 Hydrogen direct injection: Optical investigation of premixed and jet-guided combustion modes. *International Journal of Hydrogen Energy* **61**, 284–295.
- MONTANARO, ALESSANDRO, ALLOCCA, LUIGI & MECCARIELLO, GIOVANNI 2024 High-pressure hydrogen jet behavior: Flow rate and inner morphology investigation. In *WCX SAE World Congress Experience*. SAE International.
- MOTHEAU, EMMANUEL & WAKEFIELD, JOHN 2020 Investigation of finite-volume methods to capture shocks and turbulence spectra in compressible flows. *Communications in Applied Mathematics and Computational Science* **15** (1), 1–36.
- NI, ZUO, DONG, QUAN, WANG, DINGWEN & YANG, XIYU 2022 Visualization research of natural gas jet characteristics with ultra-high injection pressure. *International Journal of Hydrogen Energy* **47**, 32473–32492.
- ONORATI, A, PAYRI, R, VAGLIECO, BM, AGARWAL, AK, BAE, C, BRUNEAX, G, CANAKCI, M, GAVAISES, M, GÜNTNER, M, HASSE, C, KOKJOHN, S, KONG, S-C, MORIYOSHI, Y, NOVELLA, R, PESYRIDIS, A, REITZ, R, RYAN, T, WAGNER, R & ZHAO, H 2022 The role of hydrogen for future internal combustion engines. *International Journal of Engine Research* **23** (4), 529–540.
- ORESCANIN, M. M., AUSTIN, J. M. & KIEFFER, S. W. 2010 Unsteady high-pressure flow experiments with applications to explosive volcanic eruptions. *Journal of Geophysical Research: Solid Earth* **115** (B6).
- POPE, STEPHEN B & POPE, STEPHEN B 2000 *Turbulent flows*. Cambridge university press.
- RAHANTAMIALISOA, FANIRY, BATTISTONI, MICHELE, MILIOZZI, ALESSIO, SAHRANAVARDFARD, NASRIN & ZEMBI, JACOPO 2023 Investigations on hydrogen injections using a real-fluid approach.
- RAHANTAMIALISOA, F. N.Z., ZEMBI, J., MILIOZZI, A., SAHRANAVARDFARD, N. & BATTISTONI, M. 2022 Cfd simulations of under-expanded hydrogen jets under high-pressure injection conditions. , vol. 2385. Institute of Physics.
- REN, ZHAOXIN & WEN, JENNIFER X. 2020 Numerical characterization of under-expanded cryogenic hydrogen gas jets. *AIP Advances* **10**.
- ROACHE, P. J. 1997 *Quantification of uncertainty in computational fluid dynamics*. Annual Review of Fluid Mechanics.
- RUGGLES, A.J. & EKOTO, I.W. 2012 Ignitability and mixing of underexpanded hydrogen jets. *International Journal of Hydrogen Energy* **37** (22), 17549–17560, hySafe 1.
- SAKELLARAKIS, V. D., VERA-TUDELA, W., DOLL, U., EBI, D., WRIGHT, Y. M. & BOULOUCHOS, K. 2021

- The effect of high-pressure injection variations on the mixing state of underexpanded methane jets. *International Journal of Engine Research* **22**, 2900–2918.
- SAMSAM-KHAYANI, HADI, CHEN, BINQI, KIM, MIRAE & KIM, KYUNG CHUN 2022 Visualization of supersonic free jet flow structures subjected to various temperature and pressure ratio conditions. *Optics and Lasers in Engineering* **158**, 107144.
- SMAGORINSKY, J. 1963 General circulation experiments with the primitive equations: I. the basic experiment. *Monthly Weather Review* **91** (3), 99 – 164.
- SU, HONGMIN, CAI, JINSHENG, QU, KUN & PAN, SHUCHENG 2020 Numerical simulations of inert and reactive highly underexpanded jets. *Physics of Fluids* **32** (3), 036104.
- TRAXINGER, CHRISTOPH, BANHOLZER, MATTHIAS & PFITZNER, MICHAEL 2018 Real-gas effects and phase separation in underexpanded jets at engine-relevant conditions .
- VUORINEN, V., WEHRFRITZ, A., DUWIG, C. & BOERSMA, B. J. 2014 Large-eddy simulation on the effect of injection pressure and density on fuel jet mixing in gas engines. *Fuel* **130**, 241–250.
- VUORINEN, V., YU, J., TIRUNAGARI, S., KAARIO, O., LARMI, M., DUWIG, C. & BOERSMA, B. J. 2013 Large-eddy simulation of highly underexpanded transient gas jets. *Physics of Fluids* (1), 016101.
- WANG, YIQING, SCARCELLI, RICCARDO, BESTEL, DIEGO, DEMIR, SINAN & SRNA, ALEŠ 2024 Multi-dimensional modeling of mixture formation in a hydrogen-fueled heavy-duty optical engine with direct injection **ASME 2024 ICE Forward Conference**, V001T06A004.
- XIAO, CHENG NIAN, FOND, BENOIT, BEYRAU, FRANK, T'JOEN, CHRISTOPHE, HENKES, RUUD, VEENSTRA, PETER & VAN WACHEM, BEREND 2019 Numerical investigation and experimental comparison of the gas dynamics in a highly underexpanded confined real gas jet. *Flow, Turbulence and Combustion* **103**, 141–173.
- YEGANEH, MARYAM, CHENG, QIANG, DHARAMSI, AISHWARYA, KARIMKASHI, SHERVIN, KUUSELA-OPAS, JUHO, KAARIO, OSSI & LARMI, MARTTI 2023a Visualization and comparison of methane and hydrogen jet dynamics using schlieren imaging. *Fuel* **331**, 125762.
- YEGANEH, MARYAM, RABENSTEINER, SAMUEL, CHENG, QIANG, RANTA, OLLI, KARIMKASHI, SHERVIN, KAARIO, OSSI & LARMI, MARTTI 2022 Experimental and numerical investigation of hydrogen jet-wall impingement. In *SAE Powertrains, Fuels & Lubricants Conference & Exhibition*. SAE International.
- YEGANEH, MARYAM, RABENSTEINER, SAMUEL, KARIMKASHI, SHERVIN, CHENG, QIANG, KAARIO, OSSI & LARMI, MARTTI 2023b Experimental and numerical study of a low-pressure hydrogen jet under the effect of nozzle geometry and pressure ratio. In *WCX SAE World Congress Experience*. SAE International.
- YOSRI, MOHAMMAD REZA, TALEI, MOHSEN, GORDON, ROBERT, BREAR, MICHAEL & LACEY, JOSHUA 2020 A numerical simulation of an under-expanded jet issued from a prototype injector. The University of Queensland.
- YU, JINGZHOU, HILLAMO, HARRI, VUORINEN, VILLE, SARJOVAARA, TEEMU, KAARIO, OSSI & LARMI, MARTTI 2011 Experimental investigation of characteristics of transient low pressure wall-impinging gas jet. , vol. 318. Institute of Physics Publishing.
- YU, JINGZHOU, VUORINEN, VILLE, KAARIO, OSSI, SARJOVAARA, TEEMU & LARMI, MARTTI 2013a Characteristics of high pressure jets for direct injection gas engine. *International Journal of Fuels and Lubricants* **6**, 149–156.
- YU, JINGZHOU, VUORINEN, VILLE, KAARIO, OSSI, SARJOVAARA, TEEMU & LARMI, MARTTI 2013b Visualization and analysis of the characteristics of transitional underexpanded jets. *International Journal of Heat and Fluid Flow* **44**, 140–154.
- ZHANG, HUAN-HAO, AUBRY, NADINE, CHEN, ZHI-HUA, WU, WEI-TAO & SHA, SHA 2019a The evolution of the initial flow structures of a highly under-expanded circular jet. *Journal of Fluid Mechanics* **871**, 305–331.
- ZHANG, HUAN-HAO, AUBRY, NADINE, CHEN, ZHI-HUA, WU, WEI-TAO & SHA, SHA 2019b The evolution of the initial flow structures of a highly under-expanded circular jet. *Journal of Fluid Mechanics* **871**, 305–331.
- ZHANG, WEIQUN, ALMGREN, ANN, BECKNER, VINCE, BELL, JOHN, BLASCHKE, JOHANNES, CHAN, CY, DAY, MARCUS, FRIESEN, BRIAN, GOTT, KEVIN, GRAVES, DANIEL, KATZ, MAX P., MYERS, ANDREW, NGUYEN, TAN, NONAKA, ANDREW, ROSSO, MICHELE, WILLIAMS, SAMUEL & ZINGALE, MICHAEL 2019c Amrex: a framework for block-structured adaptive mesh refinement. *Journal of Open Source Software* **4** (37), 1370.